A Biophysically Based Mathematical Model for the Kinetics of Mitochondrial Na$^+$-Ca^{2+} Antiporter

Ranjan K. Pradhan, Daniel A. Beard, and Ranjan K. Dash*
Biotechnology and Bioengineering Center and Department of Physiology, Medical College of Wisconsin, Milwaukee, Wisconsin

ABSTRACT   Sodium-calcium antiporter is the primary efflux pathway for Ca^{2+} in respiring mitochondria, and hence plays an important role in mitochondrial Ca^{2+} homeostasis. Although experimental data on the kinetics of Na$^+$-Ca^{2+} antiporter are available, the structure and composition of its functional unit and kinetic mechanisms associated with the Na$^+$-Ca^{2+} exchange (including the stoichiometry) remains unclear. To gain a quantitative understanding of mitochondrial Ca^{2+} homeostasis, a biophysical model of Na$^+$-Ca^{2+} antiporter is introduced that is thermodynamically balanced and satisfactorily describes a number of independent data sets under a variety of experimental conditions. The model is based on a multistate catalytic binding mechanism for carrier-mediated facilitated transport and Eyring's free energy barrier theory for interconversion and electrodiffusion. The model predicts the activating effect of membrane potential on the antiporter function for a 3Na$^+$:1Ca^{2+} electrogenic exchange as well as the inhibitory effects of both high and low pH seen experimentally. The model is useful for further development of mechanistic integrated models of mitochondrial Ca^{2+} handling and bioenergetics to understand the mechanisms by which Ca^{2+} plays a role in mitochondrial signaling pathways and energy metabolism.

INTRODUCTION

Calcium is a key regulatory ion, and alteration of mitochondrial Ca^{2+} homeostasis can lead to mitochondrial dysfunction and cellular injury (1–5). Despite the recognized role of Ca^{2+} in mitochondrial bioenergetics and cell physiology and pathophysiology, there are still significant gaps in our understanding of the structure, composition, and kinetic properties of the mitochondrial Ca^{2+} transport systems (e.g., Na$^+$-Ca^{2+} antiporter).

The Na$^+$-Ca^{2+} antiporter mediates Ca^{2+} efflux from mitochondria in exchange of Na$^+$ from cytosol, and hence plays a key role in mitochondrial Ca^{2+} homeostasis (1,4). This Na$^+$ influx (Ca^{2+} efflux) is inhibited by both high and low pH with peak activity near pH = 7.0–7.3 (6,7). Although this Na$^+$-dependent Ca^{2+} exchange has been characterized in a number of experimental studies (6–15), the kinetic mechanism associated with the exchange has not been well characterized as a mechanistic model that can account for thermodynamics of the exchange process and other physiochemical mechanisms such as allosteric, cooperative binding of Na$^+$ to the antiporter and competitive binding and inhibition by other cations (e.g., H$^+$). Another important point is that the stoichiometry of the exchange is not well known. A number of reports indicate that the exchange is electroneutral (7,9,15): 2Na$^+$ for 1Ca^{2+}. Other reports indicate an electrogenic (perhaps 3Na$^+$ for 1Ca^{2+}) exchange (8,13,16). Therefore, the need for a mechanistic model of the antiporter is apparent for quantitative understanding of mitochondrial Ca^{2+} handling and bioenergetics and determining the stoichiometry of the exchange.

Magnus and Keizer (17) developed a kinetic model of the Na$^+$-Ca^{2+} antiporter from the experimental data of Wingrove and Gunter (15) as a module of an integrated model of mitochondrial energy metabolism and Ca^{2+} handling in pancreatic β-cells. The model was based on a single-step binding mechanism of nNa$^+$ and 1Ca^{2+} to the antiporter and a phenomenological, irreversible Goldman-Hodgkin-Katz constant-field approximation for electrodiffusion. The model was adopted by Cortassa et al. (18) in their computational models of mitochondrial energy metabolism and Ca^{2+} dynamics in cardiomyocytes. However, the Magnus-Keizer model is not thermodynamically balanced, as it collapses for membrane potential $\Delta\Psi \leq \Delta\Psi* = 91$ mV.

In part to address the limitations of the Magnus-Keizer model, Nguyen et al. (19) developed another model of the antiporter as a module of a computational model of mitochondrial bioenergetics and Ca^{2+} dynamics in cardiomyocytes. The model was based on a random-ordered, bi-bi binding mechanism of 3Na$^+$ for 1Ca^{2+} to the antiporter and a reversible Goldman-Hodgkin-Katz equation for electrodiffusion, which makes the model thermodynamically balanced. Recently, this model was adopted by Dash and Beard (16) in their integrated model of mitochondrial bioenergetics and Ca^{2+} handling, in which they generalized the model to both 2Na$^+$:1Ca^{2+} and 3Na$^+$:1Ca^{2+} stoichiometries to evaluate the actual stoichiometry of the antiporter, based on the dynamic data of Cox and Matlib (12) on matrix free [Ca^{2+}] with extramatrix [Na$^+$] perturbations in isolated respiring cardiac mitochondria. The two antiporter models were parameterized based on the kinetic data of Paucek and Jaburek (7) on Na$^+$-Ca^{2+} fluxes, obtained using proteoliposomes reconstituted with purified cardiac mitochondrial Na$^+$-Ca^{2+} antiporters. However, as these data were obtained with $\Delta\Psi = 0$, the $\Delta\Psi$-dependency of the antiporter function

was not mechanistically incorporated into the model for a $3Na^+:1Ca^{2+}$ exchange. In a recent study, Kim and Matsuoka (14) developed another model of the antiporter, driven by their data showing the $\Delta\Psi$-dependency of the exchange in isolated permeabilized cardiomyocytes. The model was based on a simplified mechanism of binding and translocation of Na^+ and Ca^{2+} via the antiporter, proposed by Crompton et al. (11). However, none of these models account for the proton inhibition of the antiporter function, observed experimentally (6,7).

In this article, we develop a mechanistic model of mitochondrial Na^+-Ca^{2+} antiporter which improves upon and generalizes our previous model (16) and provides a biophysical basis for the $\Delta\Psi$-dependency of the antiporter function for a $3Na^+:1Ca^{2+}$ exchange. The model is thermodynamically balanced and adequately describes the independent data of Paucek and Jaburek (7), Cox and Matlib (12), and Kim and Matsuoka (14) on Na^+-Ca^{2+} fluxes via the antiporter. In addition, the model predicts the inhibitory effects of both high and low pH on the antiporter function, seen experimentally (6,7), making the model applicable to pathological conditions, in which the extra- and intramatrix pH vary considerably. The model is based on Michaelis-Menten kinetics for carrier-mediated facilitated transport (20) and Eyring's free energy barrier theory for absolute reaction rates associated with the conformational change and electrodiffusion of the nNa^+- and $1Ca^{2+}$-bound carrier complex (20–22).

MATHEMATICAL FORMULATION

Experimental data for model development and validation

Experimental data on the kinetics of mitochondrial Na^+-dependent Ca^{2+} exchange are available from a number of studies (6–15). These data include the initial or pseudo-steady rate data on Na^+-Ca^{2+} fluxes via the antiporter as well as the time-course data on matrix free $[Ca^{2+}]$ with extramatrix $[Na^+]$ perturbations in isolated respiring mitochondria and permeabilized myocytes. However, the time-course data on matrix free $[Ca^{2+}]$, which represent an integrated response of cation transport system, are not ideally suited to developing kinetic models of individual cation transporters (e.g., Na^+-Ca^{2+} antiporter). For development of a kinetic model of a cation transporter, the initial or pseudo-steady rate data on cation fluxes via the transporter are more useful. Therefore, the initial rate data of Paucek and Jaburek (7), Cox and Matlib (12), and Kim and Matsuoka (14) on Na^+-Ca^{2+} fluxes via mitochondrial Na^+-Ca^{2+} antiporter are chosen for the development of kinetic model of the antiporter.

Paucek and Jaburek report the initial rate of Na^+ efflux (Ca^{2+} influx) in response to variations in external $[Ca^{2+}]$ and initial rate of Ca^{2+} efflux (Na^+ influx) in response to variations in external $[Na^+]$ using proteoliposomes reconstituted with purified Na^+-Ca^{2+} antiporters from beef heart

mitochondria. These data also reveal inhibition of Na^+-Ca^{2+} fluxes by both high and low pH with optimal activity near pH = 7.0–7.3. However, these data were obtained without an electrostatic potential across the proteoliposomes. In contrast, the data of Cox and Matlib describe the initial rate of decrease of matrix free $[Ca^{2+}]$ in response to addition of Na^+ to the suspensions of respiring mitochondria from rabbit heart with Ca^{2+} uniporter blocked. Furthermore, the data of Kim and Matsuoka show the Na^+ dependency of Ca^{2+} extrusion from the matrix, in which the Na^+-Ca^{2+} fluxes and matrix free $[Ca^{2+}]$ dynamics were measured with varying extramatrix $[Na^+]$ in permeabilized cardiomyocytes during state-2 respiration. These data suggest a $\Delta\Psi$-dependent electrogenic exchange of $3Na^+:1Ca^{2+}$ via the antiporter. Our proposed kinetic model is based on basic physical-chemical principles and parameterized to accurately reproduce the data of Paucek and Jaburek, Cox and Matlib, and Kim and Matsuoka.

Mechanism of Na^+-dependent Ca^{2+} exchange in mitochondria

Using the available data on Na^+-dependent Ca^{2+} efflux from the matrix, a mathematical model for the kinetics of Na^+-Ca^{2+} antiporter is developed using a multistate catalytic binding and interconversion mechanism and Eyring's free energy barrier theory for absolute reaction rates (20–22). Fig. 1 schematizes the proposed kinetic mechanism for a $3Na^+:1Ca^{2+}$ exchange via the antiporter. The $2Na^+:1Ca^{2+}$ exchange can be similarly developed (see Supporting Material).

The functional unit of the antiporter (E) is assumed to have three binding sites for Na^+ and one binding site for Ca^{2+} on either side of the inner mitochondrial membrane (IMM). The binding of Na^+ and Ca^{2+} to the antiporter is assumed to be via a random-ordered mechanism (e.g., a random-ordered, bi-bi mechanism when three Na^+ ions are considered to bind in a single step). If an ionized Na^+ from the external side first binds to the unbound antiporter (E) to form the complex ENa_e^+ it then favors binding of another ionized Na^+ forming the complex $E2Na_e^+$, which further favors the binding of a third ionized Na^+ to form the complex $E3Na_e^+$. Then an ionized Ca^{2+} from the internal side binds to the complex $E3Na_e^+$ to form the complex $Ca_x^{2+}E3Na_e^+$. On the other hand, if an ionized Ca^{2+} from the internal side first binds to the unbound antiporter (E) to form the complex Ca_x^{2+}, it then favors cooperative binding of three ionized Na^+ from the external side in three consecutive steps to form the same complex $Ca_x^{2+}E3Na_e^+$. The complex $Ca_x^{2+}E3Na_e^+$ then undergoes a conformational change to form the complex $3Na_x^+ECa_e^{2+}$. The complex $3Na_x^+ECa_e^{2+}$ then dissociates three ionized Na^+ in the internal side and one ionized Ca^{2+} in the external side, along with the unbound antiporter (E), by going through the reverse process. The complexes $Ca_x^{2+}E2Na_e^+$, $2Na_x^+ECa_e^{2+}$, $Ca_x^{2+}ENa_e^+$, and $Na_x^+ECa_e^{2+}$ are assumed not to undergo any conformational flipping. The
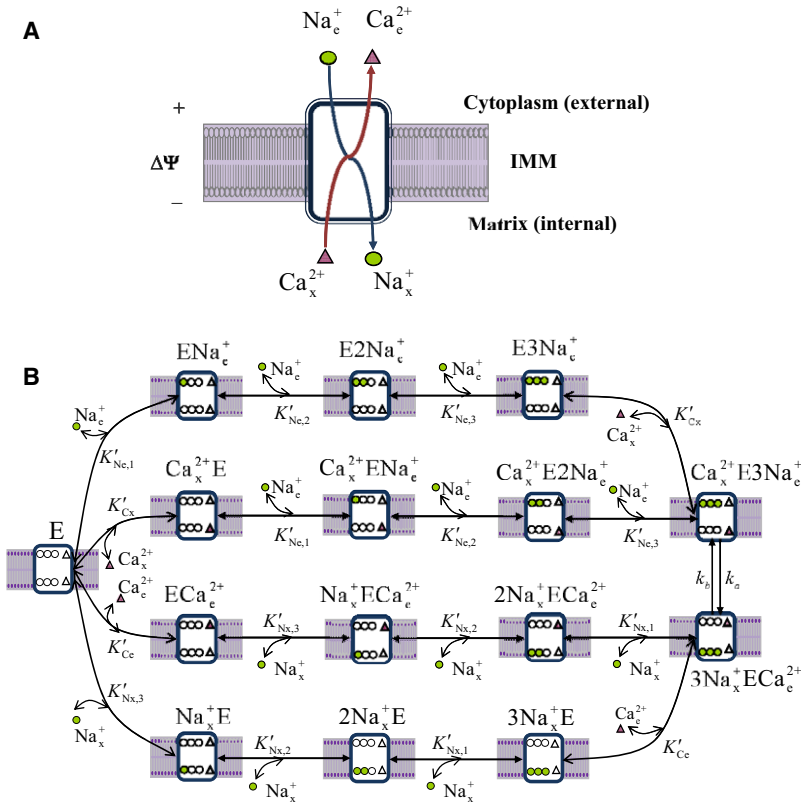
A

B

FIGURE 1   (*A, B*) Proposed kinetic mechanism of Na^+-dependent Ca^{2+} efflux from mitochondria via Na^+-Ca^{2+} antiporter with a presumed $3Na^+$:$1Ca^{2+}$ stoichiometry. The antiporter E has three binding sites for Na^+ and one binding site for Ca^{2+} facing either side of the IMM. In one process, three Na^+ ions from cytoplasmic side first cooperatively bind to the unbound antiporter E in three consecutive steps to form the complex $E3Na_e^+$. Then one Ca^{2+} ion from the matrix side binds to the complex $E3Na_e^+$ to form the complex $Ca_x^{2+}E3Na_e^+$. In another process, one Ca^{2+} ion from the matrix side first binds to the unbound antiporter E to form the complex $Ca_x^{2+}E$. Then three Na^+ ions from the cytoplasmic side cooperatively bind to the complex $Ca_x^{2+}E$ in three consecutive steps to form the complex $Ca_x^{2+}E3Na_e^+$. The complex $Ca_x^{2+}E3Na_e^+$ then undergoes conformational changes to form the complex $3Na_x^+ECa_e^{2+}$. The complex $3Na_x^+ECa_e^{2+}$ then undergoes the reverse processes, where it dissociates in two distinct processes to form three Na^+ ions in the matrix side and one Ca^{2+} ion in the cytoplasmic side, in addition to the unbound antiporter E. $K'_{Ne,\ p}$, $K'_{Nx,\ p}$, K'_{Ce}, and K'_{Cx} are the apparent dissociation constants associated with the binding of external and internal Na^+ and Ca^{2+} to the antiporter. The $3Na^+$:$1Ca^{2+}$ exchange via the interconversion mechanism $Ca_x^{2+}E3Na_e^+ \leftrightarrow 3Na_x^+ECa_e^{2+}$ is limited by the forward and reverse rate constants k_a and k_b, which depend on $\Delta\Psi$.

exchange of $3Na^+$ for $1Ca^{2+}$ is limited by the interconversion rate constants k_a and k_b, which are functions of $\Delta\Psi$.

Derivation of mitochondrial Na^+-Ca^{2+} antiporter flux expression

Based on the proposed kinetic mechanism (Fig. 1) and the assumption of quasisteady flux and rapid equilibrium binding of external and internal Na^+ and Ca^{2+} to the antiporter, the binding and translocation reactions for a general nNa^+-$1Ca^{2+}$ antiporter can be summarized as
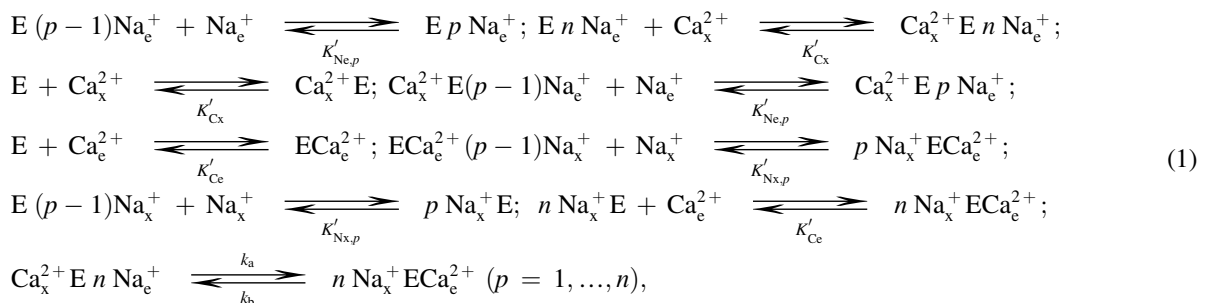
the stoichiometry (e.g., $n = 3$ represents a $3Na^+$:$1Ca^{2+}$ antiporter); and the dissociation constants are ($K'_{Ne,1}$, $K'_{Nx,1}$, $K'_{Ne,2}$, $K'_{Nx,2}$, $K'_{Ne,3}$, $K'_{Nx,3}$, K'_{Ce}, and K'_{Cx}). The values (k_a, k_b) are the forward and reverse rate constants in the interconversion of the antiporter complexes $Ca_x^{2+}EnNa_e^+$ and $nNa_x^+ECa_e^{2+}$. Due to translocation of positive charges across the IMM, the rate constants (k_a, k_b) are functions of $\Delta\Psi$. Depending on the physical locations of Na^+ and Ca^{2+} binding sites on the antiporter, the dissociation constants ($K'_{Ne,\ p}$, $K'_{Nx,\ p}$, K'_{Ce}, and K'_{Cx}) may also depend on $\Delta\Psi$.

$$
\begin{aligned}
&E\,(p-1)Na_e^+ + Na_e^+ \xrightleftharpoons[K'_{Ne,p}]{} E\,p\,Na_e^+; \quad E\,n\,Na_e^+ + Ca_x^{2+} \xrightleftharpoons[K'_{Cx}]{} Ca_x^{2+}E\,n\,Na_e^+; \\[4pt]
&E + Ca_x^{2+} \xrightleftharpoons[K'_{Cx}]{} Ca_x^{2+}E; \quad Ca_x^{2+}E(p-1)Na_e^+ + Na_e^+ \xrightleftharpoons[K'_{Ne,p}]{} Ca_x^{2+}E\,p\,Na_e^+; \\[4pt]
&E + Ca_e^{2+} \xrightleftharpoons[K'_{Ce}]{} ECa_e^{2+}; \quad ECa_e^{2+}(p-1)Na_x^+ + Na_x^+ \xrightleftharpoons[K'_{Nx,p}]{} p\,Na_x^+ECa_e^{2+}; \\[4pt]
&E\,(p-1)Na_x^+ + Na_x^+ \xrightleftharpoons[K'_{Nx,p}]{} p\,Na_x^+E; \quad n\,Na_x^+E + Ca_e^{2+} \xrightleftharpoons[K'_{Ce}]{} n\,Na_x^+ECa_e^{2+}; \\[4pt]
&Ca_x^{2+}E\,n\,Na_e^+ \xrightleftharpoons[k_b]{k_a} n\,Na_x^+ECa_e^{2+} \quad (p=1,\ldots,n),
\end{aligned}
\tag{1}
$$

where ($K'_{Ne,\ p}$, $K'_{Nx,\ p}$, K'_{Ce}, and K'_{Cx}) are the apparent dissociation constants associated with the binding of external and internal Na^+ and Ca^{2+} to the antiporter; n is

Applying rapid equilibrium binding approximations, we have the following relationships between various states of the antiporter,

$$[E \, p \, Na_e^+] = \frac{[Na^+]_e^p}{\prod\limits_{i=1}^{p} K'_{Ne,i}}[E]; \quad [Ca_x^{2+} E] = \frac{[Ca^{2+}]_x}{K'_{Cx}}[E]; \quad [Ca_x^{2+} E \, p \, Na_e^+] = \frac{[Ca^{2+}]_x [Na^+]_e^p}{K'_{Cx} \prod\limits_{i=1}^{p} K'_{Ne,i}}[E];$$

$$[p \, Na_x^+ E] = \frac{[Na^+]_x^p}{\prod\limits_{i=1}^{p} K'_{Nx,i}}[E]; \quad [ECa_e^{2+}] = \frac{[Ca^{2+}]_e}{K'_{Ce}}[E]; \quad [p \, Na_x^+ ECa_e^{2+}] = \frac{[Ca^{2+}]_e [Na^+]_x^p}{K'_{Ce} \prod\limits_{i=1}^{p} K'_{Nx,i}}[E]; \tag{2}$$

where the concentrations of various antiporter states are expressed with respect to matrix volume, and $[Na^+]_e$, $[Na^+]_x$, $[Ca^{2+}]_e$, and $[Ca^{2+}]_x$ denote the extramatrix and matrix concentrations of Na^+ and Ca^{2+}. As the total antiporter concentration is constant, we have

$$[E]_{Tot} = [E] + \sum_{p=1}^{n} [E \, p \, Na_e^+] + [Ca_x^{2+} E]$$
$$+ \sum_{p=1}^{n} [Ca_x^{2+} E \, p \, Na_e^+] + \sum_{p=1}^{n} [p \, Na_x^+ E]$$
$$+ [ECa_e^{2+}] + \sum_{p=1}^{n} [p \, Na_x^+ ECa_e^{2+}]. \tag{3}$$

By substituting Eq. 2 into Eq. 3 and rearranging, the concentration of unbound antiporter ($[E]$) can be expressed in terms of the concentration of total antiporter ($[E]_{Tot}$) as

$$[E] = [E]_{Tot}/D, \tag{4}$$

where

$$D = 1 + \sum_{p=1}^{n} \frac{[Na^+]_e^p}{\prod\limits_{i=1}^{p} K'_{Ne,i}} + \frac{[Ca^{2+}]_x}{K'_{Cx}}$$
$$+ \sum_{p=1}^{n} \frac{[Ca^{2+}]_x [Na^+]_e^p}{K'_{Cx} \prod\limits_{i=1}^{p} K'_{Ne,i}} + \sum_{p=1}^{n} \frac{[Na^+]_x^p}{\prod\limits_{i=1}^{p} K'_{Nx,i}} \tag{5}$$
$$+ \frac{[Ca^{2+}]_e}{K'_{Ce}} + \sum_{p=1}^{n} \frac{[Ca^{2+}]_e [Na^+]_x^p}{K'_{Ce} \prod\limits_{i=1}^{p} K'_{Nx,i}}.$$

Based on the proposed mechanism of Na^+-dependent Ca^{2+} exchange via the antiporter (Fig. 1), the rate of nNa^+: $1Ca^{2+}$ exchange can be expressed as

$$J_{NCE} = k_a [Ca_x^+ E n \, Na_e^+] - k_b [n \, Na_x^+ ECa_e^{2+}]$$
$$= \frac{[E]_{Tot}}{D} \left(k_a \frac{[Ca^{2+}]_x [Na^+]_e^n}{K'_{Cx} \prod\limits_{i=1}^{n} K'_{Ne,i}} - k_b \frac{[Ca^{2+}]_e [Na^+]_x^n}{K'_{Ce} \prod\limits_{i=1}^{n} K'_{Nx,i}} \right). \tag{6}$$

The generalized nNa^+-$1Ca^{2+}$ antiporter flux expression (6) contains n pairs of dissociation constants for Na^+ binding

and a pair of dissociation constants for Ca^{2+} binding ($K'_{Ne, p}$, $K'_{Nx, p}$, K'_{Ce}, and K'_{Cx}; $p = 1,\ldots,n$) as well as two rate constants (k_a, k_b), resulting in a total of $2n+4$ unknown parameters. When $n = 3$, a total of 10 unknown parameters appears in the flux expression. Further reduction in the number of unknown parameters is obtained under the following assumptions.

Model 1

In one version of the model, the dissociation constant associated with the pth binding step ($K'_{Ne, p}, K'_{Nx, p}; p < n$) is assumed to be arbitrarily large with the constraints $\prod_{p=1}^{n} K'_{Ne, p} = K'^n_{Ne}$ and $\prod_{p=1}^{n} K'_{Nx, p} = K'^n_{Nx}$, which are finite (maximal cooperativity). This is valid when $K'_{Ne, p} \gg 1 \, \mu M, \ldots K'_{Ne, n} \ll 1 \, \mu M$ and $K'_{Nx, p} \gg 1 \, \mu M, \ldots K'_{Nx, n} \ll 1 \, \mu M$.

Model 2

In another version of the model, the dissociation constants associated with the binding of external and internal Na^+ are assumed to be equal to each other: $K'_{Ne, 1} = K'_{Ne, 2} \ldots = K'_{Ne, n} = K'_{Ne}$ and $K'_{Nx, 1} = K'_{Nx, 2} \ldots = K'_{Nx, n} = K'_{Nx}$ (partial cooperativity).

Model 3

In the final version of the model, the dissociation constants associated with the binding of external and internal Na^+ are assumed to satisfy the constraints: $K'_{Ne, p} = (n - p + 1) K'_{Ne}/p$ and $K'_{Nx, p} = (n - p + 1) K'_{Nx}/p$; $p = 1,2,\ldots n$ (no cooperativity).

With these three assumptions, the flux expression (6) is reduced to

$$J_{NCE} = \frac{[E]_{Tot}}{D} \left(k_a \frac{[Ca^{2+}]_x [Na^+]_e^n}{K'_{Cx} K'^n_{Ne}} - k_b \frac{[Ca^{2+}]_e [Na^+]_x^n}{K'_{Ce} K'^n_{Nx}} \right), \tag{7}$$

where

$$D = D_1 = 1 + \frac{[Na^+]_e^n}{K'^n_{Ne}} + \frac{[Ca^{2+}]_x}{K'_{Cx}} + \frac{[Ca^{2+}]_x [Na^+]_e^n}{K'_{Cx} K'^n_{Ne}}$$
$$+ \frac{[Na^+]_x^n}{K'^n_{Nx}} + \frac{[Ca^{2+}]_e}{K'_{Ce}} + \frac{[Ca^{2+}]_e [Na^+]_x^n}{K'_{Ce} K'^n_{Nx}}, \tag{8a}$$

$$D = D_2 = 1 + \sum_{p=1}^{n} \frac{\left[Na^+\right]_e^p}{K_{Ne}^{'p}} + \frac{\left[Ca^{2+}\right]_x}{K_{Cx}^{'}}$$

$$+ \sum_{p=1}^{n} \frac{\left[Ca^{2+}\right]_x \left[Na^+\right]_e^p}{K_{Cx}^{'} K_{Ne}^{'p}} + \sum_{p=1}^{n} \frac{\left[Na^+\right]_x^p}{K_{Nx}^{'p}} + \frac{\left[Ca^{2+}\right]_e}{K_{Ce}^{'}} \quad (8b)$$

$$+ \sum_{p=1}^{n} \frac{\left[Ca^{2+}\right]_e \left[Na^+\right]_x^p}{K_{Ce}^{'} K_{Nx}^{'p}},$$

$$D = D_3 = 1 + \sum_{p=1}^{n} \frac{\left[Na^+\right]_e^p}{K_{Ne}^{'p} \prod_{i=1}^{p} \left(\frac{n-i+1}{i}\right)} + \frac{\left[Ca^{2+}\right]_x}{K_{Cx}^{'}}$$

$$+ \sum_{p=1}^{n} \frac{\left[Ca^{2+}\right]_x \left[Na^+\right]_e^p}{K_{Cx}^{'} K_{Ne}^{'p} \prod_{i=1}^{p} \left(\frac{n-i+1}{i}\right)} + \sum_{p=1}^{n} \frac{\left[Na^+\right]_x^p}{K_{Nx}^{'p} \prod_{i=1}^{p} \left(\frac{n-i+1}{i}\right)} \quad (8c)$$

$$+ \frac{\left[Ca^{2+}\right]_e}{K_{Ce}^{'}} + \sum_{p=1}^{n} \frac{\left[Ca^{2+}\right]_e \left[Na^+\right]_x^p}{K_{Ce}^{'} K_{Nx}^{'p} \prod_{i=1}^{p} \left(\frac{n-i+1}{i}\right)}.$$

Note that $\prod_{i=1}^{n}(n-i+1/i) = 1$. In each of the three variant models, the reduced flux expression contains only four binding constants ($K_{Ne}^{'}$, $K_{Nx}^{'}$, $K_{Ce}^{'}$, and $K_{Cx}^{'}$) and two rate constants (k_a, k_b), for a total of six unknown parameters. Therefore, the three different assumptions on the kinetic mechanism considerably simplify the model. The denominators D_1, D_2, and D_3 in the three reduced flux expressions contain an equal number of unknown parameters and unambiguously account for various kinetic states of the antiporter. D_2 and D_3 look more complex than D_1 due to the nature of the assumption on the kinetic mechanism. Therefore, the three variant models are the three possible minimal models of the antiporter. Even if all three models are able to fit to the same data, the estimates of parameters from these models are expected to differ. Moreover, Model 1 reproduces our previous model (16) with $k_a = \exp(+0.5(n - 2)F\Delta\Psi/RT)$, $k_b = \exp(-0.5(n - 2)F\Delta\Psi/RT)$, $K_{Ce}^{'} = K_{Cx}^{'} = K_C^{'}$, and $K_{Ne}^{'} = K_{Nx}^{'} = K_N^{'}$ (both independent of $\Delta\Psi$).

Kinetic constraint

Under equilibrium conditions, the net $nNa^+:1Ca^{2+}$ exchange flux is zero ($J_{NCE} = 0$). Thus, the kinetic parameters ($K_{Ne}^{'}$, $K_{Nx}^{'}$, $K_{Ce}^{'}$, k_a, and k_b) are further constrained by the relationship

$$\frac{k_a}{k_b} \frac{K_{Ce}^{'}}{K_{Cx}^{'}} \frac{K_{Nx}^{'n}}{K_{Nx}^{'n}} = \left(\frac{\left[Ca^{2+}\right]_e \left[Na^+\right]_x^n}{\left[Ca^{2+}\right]_x \left[Na^+\right]_e^n}\right)_{eq} = K_{eq}^{'}, \quad (9)$$

where $K_{eq}^{'}$ is the apparent equilibrium constant for the exchange of nNa^+ for $1Ca^{2+}$ via the antiporter, which is a function of pH and $\Delta\Psi$. Given this constraint, the number of unknown parameters is further reduced by one (from six to five).

Effect of pH on mitochondrial Na$^+$-Ca^{2+} antiporter function

Experimental studies suggest that Na$^+$-Ca^{2+} antiporter is regulated by protons (H$^+$) on either side of the IMM (6,7). Specifically, these studies reveal that the flux of Na$^+$ or Ca^{2+} via the antiporter is inhibited by both low and high pH with the minimal effect at an approximate pH = 7.0–7.3. Furthermore, the studies of Paucek and Jaburek (7) suggest that the H$^+$ ions inhibit the antiporter function by exclusively influencing the affinity of Ca^{2+} binding $K_C^{'}$), without influencing the affinity of Na$^+$ binding ($K_N^{'}$) or the rate constants (k_a, k_b).

We propose a kinetic mechanism to describe the pH-dependent regulation of Na$^+$ and Ca^{2+} fluxes via the antiporter (Fig. 2). This is similar to the theory of dibasic acid in enzyme kinetics (23), in which the enzyme is known to become active when a proton is bound at an allosteric site of the enzyme. Otherwise, the enzyme is inactive. In the proposed scheme, H$^+$ ions are assumed to influence the Ca^{2+} binding steps associated with the unbound antiporter E and Na$^+$-bound antiporter complexes (EnNa^+_e and nNa^+_xE) on either side of the IMM. Specifically, each antiporter state C (C: E, EnNa^+_e, and nNa^+_xE) is assumed to have multiple ($2m$, m is unknown) proton binding groups and that only one proton binding group (CmH$^+$) can bind to a Ca^{2+} ion (active). Other proton binding groups are assumed to have zero affinity for Ca^{2+} (inactive).

Based on this kinetic mechanism, the rate of nNa$^+:1$Ca^{2+} exchange can be written as

$$J_{NCE} = \frac{[E]_{Tot}}{D} \left(k_a D_{Hx} \frac{\left[Ca^{2+}\right]_x \left[Na^+\right]_e^n}{K_{Cx}^{'} K_{Ne}^{'n}} \right.$$

$$\left. - k_b D_{He} \frac{\left[Ca^{2+}\right]_e \left[Na^+\right]_x^n}{K_{Ce}^{'} K_{Nx}^{'n}} \right), \quad (10)$$

where

$$D = D_1 = D_{Hx} \left(1 + \frac{\left[Na^+\right]_e^n}{K_{Ne}^{'n}} + \frac{\left[Ca^{2+}\right]_x}{K_{Cx}^{'}} + \frac{\left[Ca^{2+}\right]_x \left[Na^+\right]_e^n}{K_{Cx}^{'} K_{Ne}^{'n}} \right)$$

$$+ D_{He} \left(1 + \frac{\left[Na^+\right]_x^n}{K_{Nx}^{'n}} + \frac{\left[Ca^{2+}\right]_e}{K_{Ce}^{'}} + \frac{\left[Ca^{2+}\right]_e \left[Na^+\right]_x^n}{K_{Ce}^{'} K_{Nx}^{'n}} \right) - 1, \quad (11a)$$

$$D = D_2 = D_{\mathrm{Hx}}\left(1 + \sum_{p=1}^{n}\frac{[\mathrm{Na}^+]_{\mathrm{e}}^{p}}{K_{\mathrm{Ne}}^{\prime p}} + \frac{[\mathrm{Ca}^{2+}]_{\mathrm{x}}}{K_{\mathrm{Cx}}^{\prime}} + \sum_{p=1}^{n}\frac{[\mathrm{Ca}^{2+}]_{\mathrm{x}}[\mathrm{Na}^+]_{\mathrm{e}}^{p}}{K_{\mathrm{Cx}}^{\prime}K_{\mathrm{Ne}}^{\prime p}}\right) + D_{\mathrm{He}}\left(1 + \sum_{p=1}^{n}\frac{[\mathrm{Na}^+]_{\mathrm{x}}^{p}}{K_{\mathrm{Nx}}^{\prime p}}\right.$$

$$\left. + \frac{[\mathrm{Ca}^{2+}]_{\mathrm{e}}}{K_{\mathrm{Ce}}^{\prime}} + \sum_{p=1}^{n}\frac{[\mathrm{Ca}^{2+}]_{\mathrm{e}}[\mathrm{Na}^+]_{\mathrm{x}}^{p}}{K_{\mathrm{Ce}}^{\prime}K_{\mathrm{Nx}}^{\prime p}}\right) - 1, \tag{11b}$$

$$D = D_3 = D_{\mathrm{Hx}}\left(1 + \sum_{p=1}^{n}\frac{[\mathrm{Na}^+]_{\mathrm{e}}^{p}}{K_{\mathrm{Ne}}^{\prime p}\prod_{i=1}^{p}\left(\frac{n-i+1}{i}\right)} + \frac{[\mathrm{Ca}^{2+}]_{\mathrm{x}}}{K_{\mathrm{Cx}}^{\prime}} + \sum_{p=1}^{n}\frac{[\mathrm{Ca}^{2+}]_{\mathrm{x}}[\mathrm{Na}^+]_{\mathrm{e}}^{p}}{K_{\mathrm{Cx}}^{\prime}K_{\mathrm{Ne}}^{\prime p}\prod_{i=1}^{p}\left(\frac{n-i+1}{i}\right)}\right)$$

$$+ D_{\mathrm{He}}\left(1 + \sum_{p=1}^{n}\frac{[\mathrm{Na}^+]_{\mathrm{x}}^{p}}{K_{\mathrm{Nx}}^{\prime p}\prod_{i=1}^{p}\left(\frac{n-i+1}{i}\right)} + \frac{[\mathrm{Ca}^{2+}]_{\mathrm{e}}}{K_{\mathrm{Ce}}^{\prime}} + \sum_{p=1}^{n}\frac{[\mathrm{Ca}^{2+}]_{\mathrm{e}}[\mathrm{Na}^+]_{\mathrm{x}}^{p}}{K_{\mathrm{Ce}}^{\prime}K_{\mathrm{Nx}}^{\prime p}\prod_{i=1}^{p}\left(\frac{n-i+1}{i}\right)}\right) - 1, \tag{11c}$$

$$D_{\mathrm{Hx}} = \left(\sum_{q=1}^{m}\frac{[\mathrm{H}^+]_{\mathrm{x}}^{q}}{K_{\mathrm{H1}}^{q}} + 1 + \sum_{q=1}^{m}\frac{K_{\mathrm{H2}}^{q}}{[\mathrm{H}^+]_{\mathrm{x}}^{q}}\right)\left(\frac{[\mathrm{H}^+]_{\mathrm{x}}^{m}}{K_{\mathrm{H2}}^{m}}\right);$$

$$D_{\mathrm{He}} = \left(\sum_{q=1}^{m}\frac{[\mathrm{H}^+]_{\mathrm{e}}^{q}}{K_{\mathrm{H1}}^{q}} + 1 + \sum_{q=1}^{m}\frac{K_{\mathrm{H2}}^{q}}{[\mathrm{H}^+]_{\mathrm{e}}^{q}}\right)\left(\frac{[\mathrm{H}^+]_{\mathrm{e}}^{m}}{K_{\mathrm{H2}}^{m}}\right), \tag{11d}$$

$$K_{\mathrm{Cx}}^{\prime} = K_{\mathrm{Cx}}\left(\sum_{q=1}^{m}\frac{[\mathrm{H}^+]_{\mathrm{x}}^{q}}{K_{\mathrm{H1}}^{q}} + 1 + \sum_{q=1}^{m}\frac{K_{\mathrm{H2}}^{q}}{[\mathrm{H}^+]_{\mathrm{x}}^{q}}\right);$$

$$K_{\mathrm{Ce}}^{\prime} = K_{\mathrm{Ce}}\left(\sum_{q=1}^{m}\frac{[\mathrm{H}^+]_{\mathrm{e}}^{q}}{K_{\mathrm{H1}}^{q}} + 1 + \sum_{q=1}^{m}\frac{K_{\mathrm{H2}}^{q}}{[\mathrm{H}^+]_{\mathrm{e}}^{q}}\right). \tag{11e}$$

Here K_{H1} and K_{H2} are the two dissociation constants associated with the binding of protons to the antiporter state C (Fig. 2); K_{C} represents the true dissociation constant for Ca^{2+} binding to the active ionized antiporter state $\mathrm{C}m\mathrm{H}^+$; $K_{\mathrm{C}}^{\prime}$ denotes the apparent dissociation constant that lumps the effect of pH, which is experimentally observable (7). We assume that K_{H1} and K_{H2} values are the same for both inside and outside of the IMM. Furthermore, as the binding of Na^+ to any antiporter state is not influenced by pH, $K_{\mathrm{Ne}}^{\prime} = K_{\mathrm{Ne}}$ and $K_{\mathrm{Nx}}^{\prime} = K_{\mathrm{Nx}}$. Incorporation of pH effects on the antiporter function introduces two more parameters, K_{H1} and K_{H2}, which are estimated separately. With this formulation, Eq. 9 is reduced to

$$\frac{k_{\mathrm{a}}}{k_{\mathrm{b}}}\frac{K_{\mathrm{Ce}}}{K_{\mathrm{Cx}}}\frac{K_{\mathrm{Nx}}^{n}}{K_{\mathrm{Ne}}^{n}} = \left(\frac{[\mathrm{Ca}^{2+}]_{\mathrm{e}}[\mathrm{Na}^+]_{\mathrm{x}}^{n}[\mathrm{H}^+]_{\mathrm{e}}^{m}}{[\mathrm{Ca}^{2+}]_{\mathrm{x}}[\mathrm{Na}^+]_{\mathrm{e}}^{n}[\mathrm{H}^+]_{\mathrm{x}}^{m}}\right)_{\mathrm{eq}} = K_{\mathrm{eq}}, \tag{12}$$

where K_{eq} is the true equilibrium constant, which is a function of $\Delta\Psi$ only. Note that when the external and internal pH become equal, Eqs. 10–12 reduce to Eqs. 7–9.

Membrane potential dependence of the kinetic parameters

The electrostatic field of the charged membrane influences the binding of Na^+ and Ca^{2+} to the antiporter and their translocation via the antiporter. To account for this dependency, we assume that the kinetics parameters K_{eq}, K_{Ne}, K_{Nx}, K_{Ce}, K_{Cx}, k_{a}, and k_{b} depend on the electrostatic potential difference $\Delta\Psi$ across the membrane. Our approach is similar to that of Metelkin et al. (24) on the kinetic modeling of mitochondrial adenine nucleotide translocase and Dash et al. (25) on the kinetic modeling of mitochondrial Ca^{2+} uniporter.

A detailed description of the approach is provided in Appendix A in the Supporting Material. We only provide here the final equations that are used to express K_{eq}, K_{Ne}, K_{Nx}, K_{Ce}, K_{Cx}, k_{a}, and k_{b} in terms of $\Delta\Psi$,

$$K_{\mathrm{eq}} = \exp[(nZ_{\mathrm{Na}} - Z_{\mathrm{Ca}})\Delta\Phi], \quad \Delta\Phi = F\Delta\Psi/RT, \tag{13}$$

$$K_{\mathrm{Ne}} = K_{\mathrm{Ne}}^0\exp(-\alpha_{\mathrm{Ne}}Z_{\mathrm{Na}}\Delta\Phi), \quad K_{\mathrm{Nx}} = K_{\mathrm{Nx}}^0\exp(+\alpha_{\mathrm{Nx}}Z_{\mathrm{Na}}\Delta\Phi),$$
$$K_{\mathrm{Ce}} = K_{\mathrm{Ce}}^0\exp(-\alpha_{\mathrm{Ce}}Z_{\mathrm{Ca}}\Delta\Phi), \quad K_{\mathrm{Cx}} = K_{\mathrm{Cx}}^0\exp(+\alpha_{\mathrm{Cx}}Z_{\mathrm{Ca}}\Delta\Phi), \tag{14}$$

$$k_{\mathrm{a}} = k_{\mathrm{a}}^0\exp[(+n\beta_{\mathrm{Ne}}Z_{\mathrm{Na}} - \beta_{\mathrm{Cx}}Z_{\mathrm{Ca}})\Delta\Phi],$$
$$k_{\mathrm{b}} = k_{\mathrm{b}}^0\exp[(-n\beta_{\mathrm{Nx}}Z_{\mathrm{Na}} + \beta_{\mathrm{Ce}}Z_{\mathrm{Ca}})\Delta\Phi], \tag{15}$$

where α_{Ne} or α_{Ce} (α_{Nx} or α_{Cx}) is the ratio of potential difference between Na^+ or Ca^{2+} bound to the site of antiporter facing the external (internal) side of the IMM and Na^+ or Ca^{2+} in the bulk phase to the total membrane potential; β_{Ne} or β_{Ce} (β_{Nx} or β_{Cx}) is the displacement of external (internal) Na^+ or Ca^{2+} from the coordinate of maximum potential barrier. For reducing the number of unknown biophysical parameters, we assume $\alpha_{\mathrm{Ne}} = \alpha_{\mathrm{Ce}} = \alpha_{\mathrm{e}}$, $\alpha_{\mathrm{Nx}} = \alpha_{\mathrm{Cx}} = \alpha_{\mathrm{x}}$,

C2mH$^+$ (Inactive)

K_{H1}

H$^+$

C(2m−1)H$^+$ (Inactive)

K_{H1} (m-1 steps)

H$^+$

(Active) CmH$^+$ + Ca^{2+} $\longleftrightarrow$ CmH$^+$Ca^{2+}
K_C

K_{H2} (m-1 steps)
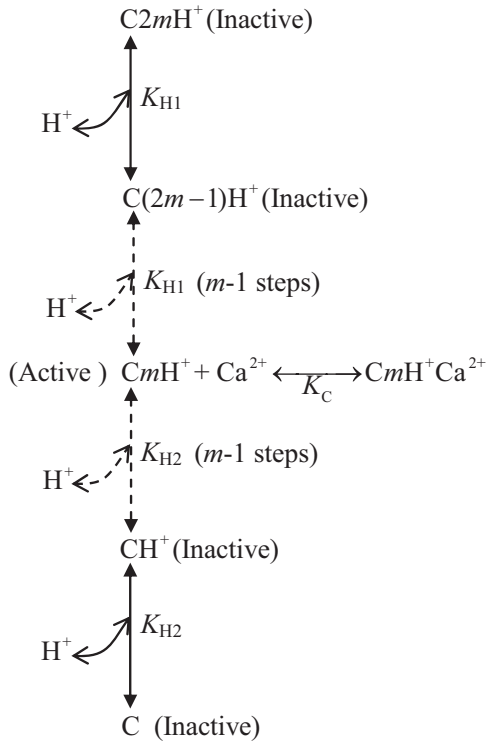
H$^+$

CH$^+$ (Inactive)

K_{H2}

H$^+$

C (Inactive)

FIGURE 2   Proposed kinetic mechanism of proton inhibition of nNa$^+$-1Ca^{2+} antiporter function. The protons are assumed to inhibit the antiporter function by their influences on Ca^{2+} binding steps, associated with the unbound antiporter E and Na$^+$-bound antiporter complexes (EnNa$^+$$_e$, nNa$^+$$_x$E) in Fig. 1, on either side of the IMM. Each antiporter state (C: E, EnNa$^+$$_e$, nNa$^+$$_x$E) is assumed to have multiple (2m) ionizable groups, but contains only one active ionizable group CmH$^+$ that can bind to a Ca^{2+} ion. The other ionizable groups are assumed to have zero affinity for Ca^{2+} (inactive). K_{H1} and K_{H2} are the two dissociation constants associated with the binding of protons to the antiporter state C; K_C represents the true dissociation constant for Ca^{2+} binding to the active ionized antiporter state CmH$^+$.

$\beta_{Ne} = \beta_{Ce} = \beta_e$, and $\beta_{Nx} = \beta_{Cx} = \beta_x$. Therefore, the four dissociation constants (K_{Ne}, K_{Nx}, K_{Ce}, K_{Cx}) and two rate constants (k_a, k_b) are fully characterized by 10 unknown parameters (K^0_{Ne}, K^0_{Nx}, K^0_{Ce}, K^0_{Cx}, K^0_a, K^0_b, α_e, α_x, β_e, and β_x; note that α_e, α_x, β_e, and β_x are estimated separately).

Kinetic and thermodynamic constraints

By substituting Eq. 13 for K_{eq}, Eq. 14 for K_{Ne}, K_{Nx}, K_{Ce}, and K_{Cx}, and Eq. 15 for k_a and k_b into Eq. 12, we obtain the following relationships, which lead to further parameter reduction by two:

$$\frac{k^0_a}{k^0_b} \frac{K^0_{Ce}}{K^0_{Cx}} \left(\frac{K^0_{Nx}}{K^0_{Ne}}\right)^n = 1, \alpha_e + \alpha_x + \beta_e + \beta_x = 1. \quad (16)$$

Statistical methods and parameter estimation

The 12 antiporter model parameters $\varphi = (K^0_{Ne}, K^0_{Nx}, K^0_{Ce}, K^0_{Cx}, K^0_a, K^0_b, K_{H1}, K_{H2}, \alpha_e, \alpha_x, \beta_e,$ and $\beta_x)$ were estimated

in a systematic manner in multiple steps by least-square fitting of the model simulated outputs to the available data,

$$\min_{\varphi} E(\varphi), \, E(\varphi) = \sum_i^{N_{exp}} \sum_j^{N_{data}} \left[\frac{J^{data}_{NCE,j} - J^{model}_{NCE,j}(\varphi)}{N_{data}\max(J^{data}_{NCE,j})}\right]^2, \quad (17)$$

where N_{exp} is the number of experiments; N_{data} is the number of data points in a particular experiment; $J^{data}_{NCE,j}$ are the data on antiporter fluxes; $J^{model}_{NCE,j}(\varphi)$ are the corresponding model outputs; and $\max(J^{data}_{NCE,j})$ is the maximum value of $J^{data}_{NCE,j}$. A MATLAB-based (The MathWorks, Natick, MA) function optimizer FMINCON is used to minimize the mean residual error $E(\varphi)$ for optimal estimation of the model parameters φ, given the constraints of Eq. 16.

Special cases

As in the experiments of Paucek and Jaburek (7), Cox and Matlib (12), and Kim and Matsuoka (14), the internal [Ca^{2+}] or [Na$^+$] was negligible compared to the external [Ca^{2+}] or [Na$^+$], we may not be able to estimate all the 12 model parameters uniquely and accurately, due to nonsensitivity of certain model parameters to the data. Therefore, we explore the parameter estimation process under two special cases: $K^0_{Ne} = K^0_{Nx}$ and $K^0_{Ce} = K^0_{Cx}$ so that $k^0_a = k^0_b$ (Case 1) and $K^0_{Ne} \neq K^0_{Nx}$ and $K^0_{Ce} \neq K^0_{Cx}$ so that $k^0_a \neq k^0_b$ (Case 2). With these simplifications and constraints of Eq. 16, the number of parameters for estimation becomes six for Case 1 and eight for Case 2.

RESULTS

The parameterization and independent validation of the three different kinetic models of 3Na$^+$-1Ca^{2+} antiporter is illustrated in this section. Specifically, the three variant kinetic models (Model 1, fully cooperativity; Model 2, partial cooperativity; and Model 3, no cooperativity) under two different model assumptions (Case 1, $K^0_{Ne} = K^0_{Nx}$, $K^0_{Ce} = K^0_{Cx}$, and $k^0_a = k^0_b$; and Case 2, $K^0_{Ne} \neq K^0_{Nx}$, $K^0_{Ce} \neq K^0_{Cx}$, and $k^0_a \neq k^0_b$) are used to simulate and fit the independent data sets of Paucek and Jaburek (7), Cox and Matlib (12), and Kim and Matsuoka (14) on the kinetics of Na$^+$-Ca^{2+} antiporter, which are shown in Figs. 3–5. The estimated model parameter values corresponding to these different model assumptions and data sets are summarized in Table 1. The corresponding analyses and parameter values for a 2Na$^+$-1Ca^{2+} antiporter are given in the Supporting Material.

Figs. 3 and 4 show the model simulations and experimental data of Paucek and Jaburek, Cox and Matlib, and Kim and Matsuoka with fixed external (cytosolic) and internal (matrix) pH. The dashed lines are the simulations from Model 1; the solid lines are the simulations from Model 2; and the dotted lines are the simulations from Model 3. The left panels of Figs. 3 and 4, A and C, show fits for Case 1, whereas the right panels of Figs. 3 and 4, B and D, show fits for Case 2.
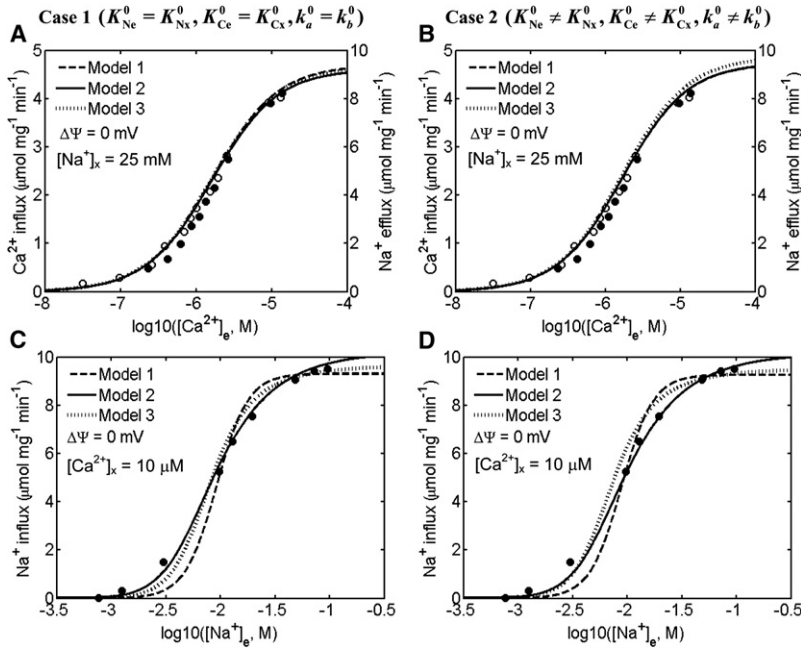
FIGURE 3 Comparison of the $3Na^+$-$1Ca^{2+}$ antiporter models (*lines*) to the experimental data (*points*) of Paucek and Jaburek (7) on the kinetics of Na^+-Ca^{2+} fluxes via the antiporter with fixed external pH. Shown are the best fits of three different kinetic models (Model 1, Model 2, and Model 3) under two different model assumptions (Case 1, (A, C); Case 2, (B, D)) to the kinetic data of Paucek and Jaburek, in which the initial rates of Ca^{2+} influx (Na^+ efflux) with variations in external $[Ca^{2+}]$ ($[Na^+]_x = 25$ mM, $[Na^+]_e = 0$ mM, $[Ca^{2+}]_x = 0$ μM, $pH_x = 7.3$, and $pH_e = 7.3$) (A, B), and the initial rates of Na^+ influx (Ca^{2+} efflux) with variations in external $[Na^+]$ ($[Na^+]_x = 0$ mM, $[Ca^{2+}]_x = 10$ μM, $[Ca^{2+}]_e = 0$ μM, $pH_x = 7.3$, and $pH_e = 7.3$) (C, D) were measured in proteoliposomes reconstituted with purified Na^+-Ca^{2+} antiporters of beef heart mitochondria. The models were fitted to the data with $\Delta\Psi = 0$ mV, in consistence with the experimental protocol. The scaling factor used to scale the model simulated Na^+ fluxes to match the data on Na^+ fluxes is $2/n = 2/3$ ($n = 3$ is the stoichiometry in nNa^+-$1Ca^{2+}$ exchange).

In one of the experiments of Paucek and Jaburek (7), the initial rates of Ca^{2+} influx (Na^+ efflux) after variations in external $[Ca^{2+}]$ were measured in proteoliposomes reconstituted with purified Na^+-Ca^{2+} antiporters of bovine heart mitochondria (Fig. 3, A and B). In another experiment, the initial rates of Na^+ influx (Ca^{2+} efflux) after variations in external $[Na^+]$ were measured in the same system (Fig. 3, C and D). The measurements were made in the absence of an electrostatic potential across the proteoliposomes. Therefore, for fitting the models to these data, the membrane potential was fixed at $\Delta\Psi = 0$ mV. In this case, the biophysical parameters $\alpha_e = \alpha_x = \alpha$ and $\beta_e = \beta_x = \beta$ can be arbitrarily chosen to satisfy the thermodynamic constraint of Eq. 16, as these parameters cannot be obtained from these $\Delta\Psi$-independent data. Nevertheless, these data provide unique and accurate estimates of the kinetic parameters K_{Ne}^0, K_{Nx}^0, K_{Ce}^0, and K_{Cx}^0, given K_{H1} and K_{H2}. However, the rate constants k_a and k_b estimated from these data differ slightly (Table 1), probably due to discrepancy in these data (Fig. 3, plots A and B, versus plots C and D). As both the external and internal mediums were maintained at a constant pH of 7.3, these data cannot provide accurate estimates of the
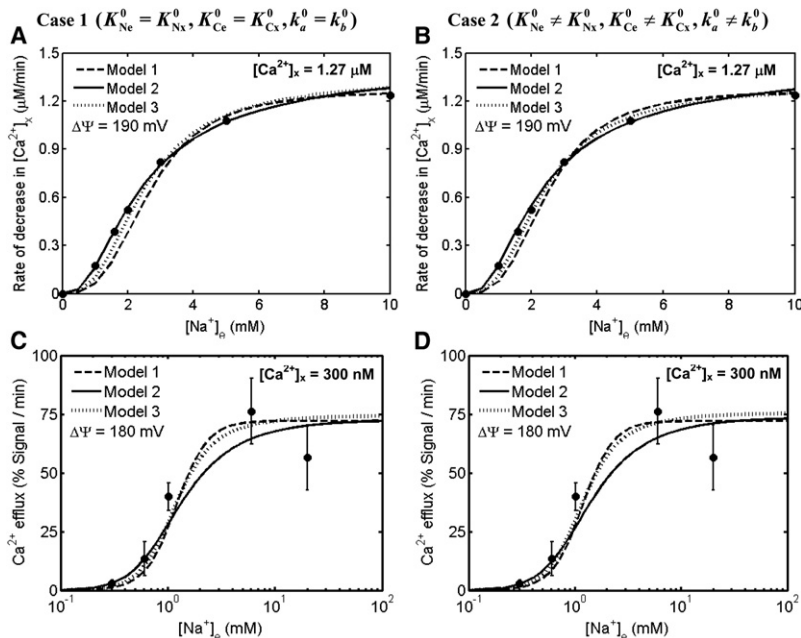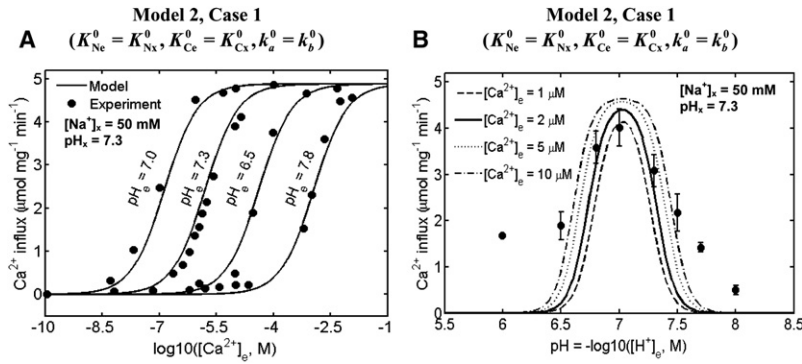

FIGURE 4 Comparison of the $3Na^+$-$1Ca^{2+}$ antiporter models (*lines*) to the experimental data (*points*) of Cox and Matlib (12) and Kim and Matsuoka (14) on the kinetics of Na^+-Ca^{2+} fluxes via the antiporter with fixed external pH. Shown are the best fits of three different kinetic models (Model 1, Model 2, and Model 3) under two different model assumptions (Case 1, (A, C); Case 2, (B, D)) to the kinetic data of Cox and Matlib in which the initial rates of decrease of matrix free $[Ca^{2+}]$ with variations in external $[Na^+]$ ($[Na^+]_e = 0$ mM, free $[Ca^{2+}]_x = 1.27$ μM, free $[Ca^{2+}]_e = 0.15$ μM, $pH_e = 7.2$, and $pH_x = 7.3$) were measured in purified mitochondria from rabbit hearts during state-2 respiration ($\Delta\Psi = 190$ mV) using fluorescence probes Fura-2 (A, B), and to the kinetic data of Kim and Matsuoka in which the initial rates of Ca^{2+} efflux (Na^+ influx) with variations in external $[Na^+]$ ($[Na^+]_x = [Na^+]_e/8.6$ mM, $[Ca^{2+}]_x = 300$ nM, $[Ca^{2+}]_e = 0$, $pH_e = 7.2$, and $pH_x = 7.3$) were measured in permeabilized cardiomyocytes during state-2 respiration ($\Delta\Psi = 180$ mV) using fluorescence probes Rhod-2 (C, D). The models were fitted to the data using the appropriate values of $\Delta\Psi$, consistent with the experimental protocols.

FIGURE 5 Comparison of the $3Na^+$-$1Ca^{2+}$ antiporter models (*lines*) to the experimental data (*points*) of Paucek and Jaburek (7) on the kinetics of Na^+-Ca^{2+} fluxes via the antiporter with varying external pH. Shown are the best fits of the best kinetic model (Model 2, Case 1) to the kinetic data of Paucek and Jaburek in which the initial rates of Ca^{2+} influx (Na^+ efflux) with (*A*) variations in external $[Ca^{2+}]$ at four different levels of external pH ($[Na^+]_x$ = 50 mM, $[Na^+]_e$ = 0 mM, $[Ca^{2+}]_x$ = 0 μM, pH_x = 7.3, and pH_e = 7.0, 7.3, 6.5, and 7.8), and (*B*) variations in external pH and fixed external $[Ca^{2+}]$ ($[Na^+]_x$ = 50 mM, $[Na^+]_e$ = 0 mM, $[Ca^{2+}]_x$ = 0 μM, $[Ca^{2+}]_e$ = 2 μM, and pH_x = 7.3) were measured in proteoliposomes reconstituted with purified Na^+-Ca^{2+} antiporters of beef heart mitochondria. Also shown in plot *B* are the model simulations of the initial rates of Ca^{2+} influx (Na^+ efflux) with variations in external pH at four different levels of external $[Ca^{2+}]$ (1, 2, 5, and 10 μM) with other experimental conditions remaining the same. The model was fitted to the data by setting $\Delta\Psi$ = 0 mV, in consistent with the experimental protocol.

proton binding constants K_{H1} and K_{H2}. However, these data provide unique and accurate estimates of the apparent binding constants K'^0_{Ce} and K'^0_{Cx} (Table 1).

In the experiment of Cox and Matlib (12), the initial rates of decrease of matrix free $[Ca^{2+}]$ after variations in external $[Na^+]$ were measured in purified mitochondria of rabbit hearts during state-2 respiration ($\Delta\Psi \approx 190$ mV) using

the fluorescence probes Fura-2 (Fig. 4, *A* and *B*). In the experiment of Kim and Matsuoka (14), the initial rates of Ca^{2+} efflux (Na^+ influx) via the antiporter after variations in external $[Na^+]$ were measured in permeabilized cardiomyocytes during state-2 respiration ($\Delta\Psi \approx 180$ mV) using the fluorescence probes Rhod-2 (Fig. 4, *C* and *D*). In contrast to the data of Paucek and Jaburek (7), these data depend on

TABLE 1   Estimated parameter values in the models of mitochondrial $3Na^+$-$1Ca^{2+}$ antiporter

Parameter	Values for Model 1		Values for Model 2		Values for Model 3		
	Case 1 ($K^0_{Ne} = K^0_{Nx}$, $K^0_{Ce} = K^0_{Cx}$)	Case 2 ($K^0_{Ne} \neq K^0_{Nx}$, $K^0_{Ce} \neq K^0_{Cx}$)	Case 1 ($K^0_{Ne} = K^0_{Nx}$, $K^0_{Ce} = K^0_{Cx}$)	Case 2 ($K^0_{Ne} \neq K^0_{Nx}$, $K^0_{Ce} \neq K^0_{Cx}$)	Case 1 ($K^0_{Ne} = K^0_{Nx}$, $K^0_{Ce} = K^0_{Cx}$)	Case 2 ($K^0_{Ne} \neq K^0_{Nx}$, $K^0_{Ce} \neq K^0_{Cx}$)	Reference
k^0_a	4.9, 5.5	4.78, 5.4	5.8, 5.8	5.55, 5.73	5.2, 5.65	4.91, 5.6	r1, r2
	6.80, 13.7	6.20, 12.10	7.8, 14.2	7.2, 12.5	7.2, 13.8	6.9, 13.2	r3, r4
k^0_b	4.9, 5.5	4.76, 5.37	5.8, 5.8	5.66, 5.85	5.2, 5.65	5.07, 5.8	r1, r2
	6.80, 13.7	5.70, 14.23	7.8, 14.2	8.5, 13.2	7.2, 13.8	8.55, 13.04	r3, r4
K^0_{Ne}	9.14×10^{-3}	8.83×10^{-3}	4.8×10^{-3}	5.18×10^{-3}	6.51×10^{-3}	5.87×10^{-3}	r1, r2
	2.2×10^{-3}	2.10×10^{-3}	1.4×10^{-3}	1.36×10^{-3}	1.90×10^{-3}	1.80×10^{-3}	r3
	1.03×10^{-3}	1.02×10^{-3}	0.66×10^{-3}	0.82×10^{-3}	0.90×10^{-3}	0.89×10^{-3}	r4
K^0_{Nx}	9.14×10^{-3}	8.82×10^{-3}	4.8×10^{-3}	4.89×10^{-3}	6.51×10^{-3}	5.76×10^{-3}	r1, r2
	2.2×10^{-3}	1.90×10^{-3}	1.4×10^{-3}	1.35×10^{-3}	1.90×10^{-3}	1.90×10^{-3}	r3
	1.03×10^{-3}	1.01×10^{-3}	0.66×10^{-3}	0.77×10^{-3}	0.90×10^{-3}	0.86×10^{-3}	r4
K^0_{Ce}	2.28×10^{-9}	2.29×10^{-9}	2.26×10^{-9}	2.29×10^{-9}	2.23×10^{-9}	2.30×10^{-9}	all
K^0_{Cx}	2.28×10^{-9}	1.89×10^{-9}	2.26×10^{-9}	1.89×10^{-9}	2.23×10^{-9}	2.10×10^{-9}	all
K'^0_{Ce} (pH = 7.0)	1.36×10^{-7}	1.37×10^{-7}	1.38×10^{-7}	1.37×10^{-7}	1.35×10^{-7}	1.43×10^{-7}	r1, r2
K'^0_{Ce} (pH = 7.3)	1.63×10^{-6}	1.70×10^{-6}	1.61×10^{-6}	1.70×10^{-6}	1.59×10^{-6}	1.71×10^{-6}	r1, r2
K'^0_{Ce} (pH = 6.5)	3.98×10^{-5}	3.92×10^{-5}	4.16×10^{-5}	3.92×10^{-5}	4.03×10^{-5}	4.27×10^{-5}	r1, r2
K'^0_{Ce} (pH = 7.8)	1.17×10^{-3}	1.22×10^{-3}	1.16×10^{-3}	1.22×10^{-3}	1.14×10^{-3}	1.23×10^{-3}	r1, r2
K'^0_{Ce} (pH = 7.2)	4.88×10^{-7}	5.08×10^{-7}	4.84×10^{-7}	5.08×10^{-7}	4.78×10^{-7}	5.11×10^{-7}	r3, r4
K'^0_{Ce} (pH = 7.3)	1.63×10^{-6}	1.40×10^{-6}	1.61×10^{-6}	1.40×10^{-6}	1.59×10^{-6}	1.56×10^{-6}	all
K_{H1}	6.45×10^{-8}	6.47×10^{-8}	6.39×10^{-8}	6.47×10^{-8}	6.41×10^{-8}	6.38×10^{-8}	all
K_{H2}	1.39×10^{-7}	1.40×10^{-7}	1.39×10^{-7}	1.40×10^{-7}	1.39×10^{-7}	1.40×10^{-7}	all
$\alpha_e = \alpha_x = \alpha$	0	0	0	0	0	0	all
$\beta_e = \beta_x = \beta$	0.5	0.5	0.5	0.5	0.5	0.5	all
	Standard physiochemical/thermodynamic parameters used in the model						
RT	Gas constant times temperature (298 K) in kJ mol^{-1}				2.5775		
F	Faraday's constant in kJ mol^{-1} mV^{-1}				0.096484		
Z_{Ca}, Z_{Na}	Valence of Ca^{2+} and Na^+ (unitless)				2, 1		

The rate constants k^0_a and k^0_b are defined as $k^0_a = [E]_{Tot} k^0_a$ and $k^0_b = [E]_{Tot} k^0_b$. The model parameters satisfy the constraints $(k^0_a/k^0_b)(K^0_{Ce}/K^0_{Cx})(K^0_{Nx}/K^0_{Ne})^3 = 1$ and $2(\alpha + \beta) = 1$. The rate constants are in the units of μmol/mg/min for Paucek and Jaburek data (7), μM/min in Cox and Matlib data (12), and % Rhod-2 signal/min for Kim and Matsuoka data (14), whereas all dissociation constants are in the units of molar (M). The references r1, r2, r3, and r4 correspond to Figs. 3 and 4, parts A–D, respectively, for each figure.

nonzero $\Delta\Psi$. Therefore, the biophysical parameters $\alpha_e = \alpha_x = \alpha$ and $\beta_e = \beta_x = \beta$ are accurately identified from these data, subject to the thermodynamic constraint of Eq. 16. In fact, we obtained the estimates $\alpha \approx 0$ and $\beta \approx 0.5$ (Table 1), consistent with the previous estimates of Dash and Beard (16). The values of Ca^{2+} binding constants K_{Ce}^0 and K_{Cx}^0 or $K_{Ce}'^0$ and $K_{Cx}'^0$ (except for pH correction) remained at values estimated from the data of Paucek and Jaburek (7). The values of Na^+ binding constants K_{Ne}^0 and K_{Nx}^0 or $K_{Ne}'^0$ and $K_{Nx}'^0$ differed from those obtained from the data of Paucek and Jaburek. These differences may be reconciled to the fact that the measured Na^+-Ca^{2+} fluxes are from different experimental systems; proteoliposomes reconstituted with purified cardiac mitochondrial Na^+-Ca^{2+} antiporter of Paucek and Jaburek versus isolated cardiac mitochondria of Cox and Matlib versus isolated permeabilized cardiomyocytes of Kim and Matsuoka. The estimated values of K_{Ne}^0 and K_{Nx}^0 are found ~1 mM, consistent with the reported values in Kim and Matsuoka (14) in isolated permeabilized cardiomyocytes and the estimated values of Dash and Beard (16) from the data of Cox and Matlib (12) in isolated cardiac mitochondria. As the external medium was maintained at a constant pH of 7.2 in both studies, these data do not provide the estimates of the proton binding constants K_{H1} and K_{H2}. Note that as the Ca^{2+} efflux (Na^+ influx) was expressed in different units ($\mu M/min$ in Cox and Matlib versus % Rhod-2 signal/min in Kim and Matsuoka), the rate constants were appropriately scaled from the previous estimates to fit to these data (Table 1).

From the fits of the models to the data (Figs. 3 and 4), it is apparent that all three kinetic models (Model 1, Model 2, and Model 3) of the antiporter under either of the conditions (Case 1 or Case 2) can adequately match the data. This indicates that all the variant models were well identified from the available data, with the parameters between the models having equal sensitivities to the data, and that the available data are not suitable to distinguish between the variant models. As the variant models were all effectively derived from the same kinetic mechanism under different assumptions, the estimated parameters expectedly varied between the models, as shown in Table 1. Nevertheless, Model 2 (where the dissociation constants associated with the binding of external and internal Na^+ to the antiporter states are assumed to be equal for each of the binding steps: $K_{Ne,1} = K_{Ne,2} = K_{Ne,3} = K_{Ne}$ and $K_{Nx,1} = K_{Nx,2} = K_{Nx,3} = K_{Nx}$) fits the data with least error. In addition, Case 1 and Case 2 are indistinguishable, as we obtain $K_{Ne}^0 \approx K_{Nx}^0$, $K_{Ce}^0 \approx K_{Cx}^0$, and $k_a^0 \approx k_b^0$ (Case 1) even with the assumptions $K_{Ne}^0 \neq K_{Nx}^0$, $K_{Ce}^0 \neq K_{Cx}^0$, and $k_a^0 \neq k_b^0$ (Case 2). We therefore consider Model 2 to be the most accurate model, i.e., the one that best describes the data compared to the other two models.

Fig. 5, A and B, shows the fits of Model 2 (Case 1) to the data of Paucek and Jaburek (7) on the kinetics of Ca^{2+} influx (Na^+ efflux) via the antiporter obtained under varying external pH and $[Ca^{2+}]$. In one of these experiments, the

initial rates of Ca^{2+} influx (Na^+ efflux) after variations in external $[Ca^{2+}]$ were measured in proteoliposomes reconstituted with purified Na^+-Ca^{2+} antiporters of beef heart mitochondria with different external pH ($pH_e = 7.0, 7.3, 6.5, 7.8$) (Fig. 5 A). In another experiment, the initial rates of Ca^{2+} influx (Na^+ efflux) after variations in external pH were measured in the same system with fixed external $[Ca^{2+}]$ of 2 μM (Fig. 5 B). The apparent K for Ca^{2+} binding (K'_C) was shifted from 0.55 ± 0.16 μM at pH 7.0, to 2.01 ± 0.16 μM at pH 7.3, to 42 ± 14 μM at pH 6.5, and to 1.0 ± 0.4 mM at pH 7.8.

To simulate the data in Fig. 5 A, the kinetic parameters K'^0_{Ne}, K'^0_{Nx}, K'^0_{Ce}, and K'^0_{Cx} were fixed at values as estimated from the data of Paucek and Jaburek (7), and the biophysical parameters $\alpha_e = \alpha_x = \alpha$ and $\beta_e = \beta_x = \beta$ were fixed as estimated from the data of Cox and Matlib (12) and Kim and Matsuoka (14). The maximum number of protons (m) that can bind to the antiporter states (C: E, $EnNa_e^+$, nNa_x^+E) was determined by trial-and-error until the model successfully reproduces the data. The models fitting to these data also provided accurate estimates of the proton binding constants K_{H1} and K_{H2}, which are used along with the estimates of the apparent binding constants K'^0_{Ce} and K'^0_{Cx} to obtain the estimates of the true binding constants K^0_{Ce} and K^0_{Cx} from Eq. 11e. The effect of varying pH on Na^+-Ca^{2+} antiporter function was found to be mediated by a shift in apparent K of Ca^{2+} (K'_C) from 0.138 μM at pH 7.0, to 1.61 μM at pH 7.3, to 41.6 μM at pH 6.5, and to 1.16 mM at pH 7.8, in consistency with the data. The values of Na^+-binding constants (K_{Ne}^0 and K_{Nx}^0) and the Na^+-Ca^{2+} exchange rate (k) remained the same.

We further validated the antiporter model by comparing the model to the data not used for parameterization. In Fig. 5 B, the model (Model 2, Case 1) with estimated parameter values is used to simulate the Ca^{2+} influx (Na^+ efflux) data of Paucek and Jaburek (7) with fixed external $[Ca^{2+}]$ and varying external pH. For model simulations, four different levels of external $[Ca^{2+}]$ (1 μM, 2 μM, 5 μM, and 10 μM) were used to test the sensitivity of the Ca^{2+} influx (Na^+ efflux) to variations in external $[Ca^{2+}]$. These simulations show that the model with an external $[Ca^{2+}] = 2$ μM does not match, accurately, the data for high and low pH (i.e., for pH < 6.5 and pH > 7.5). This is due to inconsistencies in the data sets in Fig. 5, A and B, in these nonphysiological ranges of pH. However, the model adequately predicts the bimodal behavior of Ca^{2+} influx (Na^+ efflux) via the antiporter with varying external pH, observed experimentally.

DISCUSSION

This article provides a detailed, systematic analysis of the kinetics of Na^+-Ca^{2+} antiporter, which is the primary pathway for Na^+-mediated Ca^{2+} extrusion in respiring mitochondria, and hence plays an important role in regulating

mitochondrial Ca^{2+}. Specifically, it presents a biophysically based, mathematical model of the antiporter, which is developed based on a multistate catalytic-binding mechanism for carrier-mediated facilitated transport [20] and Eyring's free energy barrier theory for interconversion and electrodiffusion [20–22], and validated based on comparison of model outputs to several independent data sets on Na^{+}-Ca^{2+} fluxes via the antiporter from the literature [7,12,14]. The model adequately describes the $\Delta\Psi$-independent data on Na^{+}-Ca^{2+} fluxes of Paucek and Jaburek [7] in proteoliposomes reconstituted with purified Na^{+}-Ca^{2+} antiporters from beef heart mitochondria as well as the $\Delta\Psi$-dependent data on Na^{+}-dependent Ca^{2+} effluxes of Cox and Matlib [12] in purified cardiac mitochondria and Kim and Matsuoka [14] in permeabilized cardiomyocytes during state-2 respiration. The model differs from the previous attempts [16–19] in that it is thermodynamically balanced and incorporates the observed pH-dependency of the antiporter function [6,7]. The generalization of the model to both $2Na^{+}$:$1Ca^{2+}$ and $3Na^{+}$:$1Ca^{2+}$ stoichiometry is another important feature, making the model accessible to study both electroneutral and electrogenic Na^{+}:$1Ca^{2+}$ exchange via the antiporter.

An important aspect of this study is modular model development. Once the kinetic model of the antiporter is derived and evaluated (with fixed matrix and extra-matrix pH), the proton inhibition mechanism of the antiporter function is incorporated into the model, requiring estimation of only two additional kinetic parameters based on additional kinetic data ($\Delta\Psi$-independent, pH-dependent) from the same system [7]. The pH-dependence is introduced here for the first time, making the model applicable to study antiporter function under pathological conditions (e.g., myocardial ischemia) in which the extra- and intramatrix pH vary considerably. Once the pH-dependence is established, the $\Delta\Psi$-dependence of the antiporter function is incorporated into the model by introducing the $\Delta\Psi$-dependence of the kinetic parameters based on biophysical theory of ion binding and translocation, making the model thermodynamically balanced. The additional parameters introduced by this theory are evaluated based on additional $\Delta\Psi$-dependent kinetic data from the same system [12,14]. As the resulting model is developed and parameterized in a modular fashion, representing many independent kinetic data sets on the antiporter function, the developed model is expected to best describe the antiporter function under both physiological and pathophysiological conditions.

There is no direct evidence regarding the structure and composition of Na^{+}-Ca^{2+} antiporter functional unit as well as the mechanism of Na^{+}-dependent Ca^{2+} efflux from mitochondria. Our model assumes the antiporter to have a general n number of Na^{+} binding sites ($n = 2$ or 3) and explores various Na^{+} binding mechanisms (fully cooperativity: Model 1, partial cooperativity: Model 2, and no cooperativity: Model 3) to determine the most possible Na^{+} binding mechanism that explains the observed data on the kinetics of

Na^{+}-Ca^{2+} exchange via the antiporter under a variety of experimental conditions. Specifically, with our model analyses of the available kinetic data [7,12,14], we are able to distinguish between three versions of the model, and show that Model 2 predicts the data more accurately compared to Model 1 and Model 3, with both $2Na^{+}$:$1Ca^{2+}$ electroneutral and $3Na^{+}$:$1Ca^{2+}$ electrogenic exchange.

The analyses of the available kinetic data [7,12,14] with three different kinetic models of the antiporter shows that for these models to fit the data, the dissociation constants associated with the binding of external and internal Na^{+} and Ca^{2+} to the antiporter in the absence of electric field ($\Delta\Psi = 0$) have to be of equal magnitudes (i.e., K_{Ne}^{0} and K_{Ce}^{0} have to be equal to K_{Nx}^{0} and K_{Cx}^{0}). In fact, we obtain the estimates $K_{Ne}^{0} \approx K_{Nx}^{0}$ and $K_{Ce}^{0} \approx K_{Cx}^{0}$ even with the assumptions $K_{Ne}^{0} \neq K_{Nx}^{0}$ and $K_{Ce}^{0} \neq K_{Cx}^{0}$ (Table 1), making the two cases (Case 1 and Case 2) indistinguishable. The estimates of the biophysical parameters $\alpha_{e} = \alpha_{x} = \alpha \approx 0$ and $\beta_{e} = \beta_{x} = \beta \approx 0.5$, which provide the best fit of the models to the data [7,12,14], suggest that:

1. The charge distribution on the antiporter during $Na^{+}(Ca^{2+})$ binding to the antiporter and $Na^{+}(Ca^{2+})$ translocation via the antiporter is linearly decreasing (increasing) along the direction of $Na^{+}(Ca^{2+})$ translocation from the outside (inside) to inside (outside) of the antiporter, and
2. The free energy barrier that impedes the $Na^{+}(Ca^{2+})$ translocation via the antiporter seems to be symmetric (because $\beta_{e} = \beta_{x} = \beta \approx 0.5$).

By considering two Na^{+} binding sites on the antiporter ($n = 2$), we are also able to fit the resulting model to the data of Paucek and Jaburek [7] (Appendix B in the Supporting Material), which suggests an electroneutral exchange of $2Na^{+}$ for Ca^{2+} via the antiporter. This indicates that these data are not suitable to identify the stoichiometry of the nNa^{+}:$1Ca^{2+}$ exchange. The data [7,12,14] that are used for model parameterization are mostly the initial Na^{+}-Ca^{2+} fluxes via the antiporter. In these experiments, matrix Na^{+} or Ca^{2+} was typically negligible compared to extramatrix Na^{+} or Ca^{2+} for various initial Na^{+} or Ca^{2+} flux measurements. As a result, these data were not adequate to fully characterize the stoichiometry of the nNa^{+}:$1Ca^{2+}$ exchange. However, with the help of an integrated model analysis of the dynamic data on matrix free $[Ca^{2+}]$ with varying extramatrix $[Na^{+}]$ in isolated respiring cardiac mitochondria [12], we are able show an electrogenic exchange of $3Na^{+}$ for Ca^{2+} via the antiporter, consistent with earlier experimental observations [8,13] and our recent model conclusion [16] (Appendix C in the Supporting Material).

The Na^{+}-Ca^{2+} antiporter model derived here is able to explain the data of Cox and Matlib [12] and Kim and Matsuoka [14] on mitochondrial Na^{+}-mediated Ca^{2+} effluxes, which are dependent on membrane potential $\Delta\Psi$ (Fig. 4),

without considering the nonphysical assumptions of previous models (17,18). In particular, these models have considered an offset potential $\Delta\Psi^*$ ($\approx$ 91 mV) and flux expressions appropriate for potential measured relative to this offset potential, and hence are not thermodynamically balanced. These models were justified based on the explanation that the electrical potential across the antiporter may not fall to zero concomitantly with the bulk membrane potential, possibly because of fixed charges producing electric field gradients localized to the antiporter. However, such models cannot be reconciled with measurements of bulk Na^+ and Ca^{2+} movement between the matrix and extramatrix space. Our biophysical model of the antiporter is able to account for the observed kinetic data based on a mechanistic formulation that is thermodynamically feasible. In doing this the singularity that occurs at $\Delta\Psi = \Delta\Psi^* \approx$ 91 mV in previous models (17,18) does not exist in our model. Furthermore, Model 1 and Case 1 of our model are analogous to the antiporter model of Dash and Beard (16) and Nguyen et al. (19) in their integrated model of mitochondrial bioenergetics and Ca^{2+} handling.

The proposed mechanism of proton inhibition on the antiporter function is one of the most striking features of this work. Our nNa^+ or $1Ca^{2+}$ antiporter model ($n = 2$ or 3), with proton inhibition mechanism incorporated, is able to explain accurately the data of Paucek and Jaburek (7) on proton inhibition of Na^+-mediated Ca^{2+} exchange via the antiporter (Fig. 5). The binding of m protons ($m = 6$) to the antiporter state C (C: E, $EnNa_e^+$, nNa_x^+E) (Fig. 2) is shown to influence the affinity of Ca^{2+} binding to the antiporter, without affecting the affinity of Na^+ binding to the antiporter and maximal nNa^+:$1Ca^{2+}$ exchange rate (Fig. 5 A). The bimodal response of the antiporter function (Ca^{2+} influx) to external pH for a given external $[Ca^{2+}]$ observed from the model simulation is consistent with the response seen experimentally (6,7) (Fig. 5 B); the inhibition of the antiporter activity is shown to be at both low and high pH with the minimal effect (optimal activity) at ~pH = 7.0.

A bell-shaped pH-dependence of enzyme activity is usually modeled based on the theory of dibasic acid (23), in which the enzyme is known to become active when a proton is bound at an allosteric site of the enzyme. Without any proton bound or with two protons bound, the enzyme is usually inactive. In the case of a Na^+-Ca^{2+} antiporter, this bell-shaped pH-dependence phenomenon seems to be somewhat complex. We tried to incorporate the proton inhibition mechanism of the antiporter function into the model by an induction process to fit the model to the transport flux data in Fig. 5, A and B. In this process, $2m$ ($m = 1, 2, 3, ...$) proton-bound states of the fully unloaded or fully nNa^+ loaded antiporter (C: E, $EnNa_e^+$, $nNa^{+x}E$) are considered, with exactly m proton-bound states, which are considered to be active for Ca^{2+} binding. Only when $m = 6$, we were able to fit the model to the data. A more appropriate mechanism of proton inhibition of the antiporter function might be that protons must bind to the

antiporter at allosteric sites to enable Na^+-Ca^{2+} exchange (active antiporter state) but also that protons competitively bind to the Ca^{2+} binding sites of the antiporter. In this case, high proton concentration will inhibit Ca^{2+} binding and low proton concentration will render the antiporter inactive. We also mention here that, as per the proposed mechanism of pH-dependence of the antiporter function, m protons are cotransported in a cycle of Na^+-Ca^{2+} exchange.

This model of nNa^+-$1Ca^{2+}$ antiporter is based on a general, random-ordered, bi-bi binding and transformation mechanism (Fig. 1). In this kinetic scheme, the probability of both the Ca^{2+} binding after, and that preceding, the binding of all nNa^+ is considered, due to lack of sufficient information about their order of binding. Various assumptions on the binding mechanism resulted in several (six) alternative minimal models, all having an equal number of unknown parameters. Alternative kinetic schemes can be formulated in which either the inner loop (Ca^{2+} binding precedes the nNa^+ binding) or the outer loop (Ca^{2+} binding follows the nNa^+ binding) in Fig. 1 can be considered. Accordingly, the denominator D in the flux expression will be modified. However, we note here that the number of unknown parameters in these two possible models would be the same as that in the proposed model of the antiporter. These models may also be able to fit the available kinetic data with appropriate changes in the parameter values, compared to the parameter values in our model. Therefore, selecting any specific mechanism or model will certainly require additional kinetic data on the antiporter function and information regarding the structure of the antiporter.

In addition to the general kinetic scheme shown in Fig. 1 and its two variant schemes described above, another possible general kinetic scheme and its two possible variant schemes for the antiporter function would be to consider the unbound antiporter E to have two conformational states E_e and E_x, depending on the orientation and the position of Ca^{2+} and nNa^+ binding sites on the external or the internal side of the IMM. Each of these models would involve two additional rate constants for this conformational change, which are distinct from the rate constants k_a and k_b for the conformational change of the fully loaded antiporter states $Ca_x^{2+}E_e nNa_e^+$ and $nNa_x^+E_x Ca_e^{2+}$. Specifically, they will not depend on the transmembrane potential $\Delta\Psi$, as no net charge is translocated via this conformational change. Therefore, applying these models would involve estimating a larger number of adjustable parameters than would be required by our model.

Present understanding of cardiomyocytes Ca^{2+} handling suggests the existence of intracellular Ca^{2+} subdomains (junctional cleft or submembrane space, where higher Na^+ or Ca^{2+} levels, compared to the average Na^+ or Ca^{2+} concentrations in the cytosol, may develop during cell excitation) (26,27). These Ca^{2+} subdomains are believed to be essential in some critical aspects of cell signaling and cell cycling. Consequently, the mitochondrial population situated near to

these Ca^{2+} subdomains is expected to have different behavior (e.g., higher Ca^{2+} uptake; also may be increased redox states and increased respiration) compared to those mitochondrial populations that are far away from these Ca^{2+} subdomains. Therefore, our biophysical model of mitochondrial Na^+-Ca^{2+} antiporter will form the basis for constructing biophysically based, integrated models of mitochondrial bioenergetics and Ca^{2+} handling (by integrating the Na^+-Ca^{2+} antiporter model to our existing models of the tricarboxylic acid cycle, oxidative phosphorylation, cation handling, and electrophysiology (28)), which may be helpful in understanding the mechanisms by which Ca^{2+} plays a role in mediating signaling pathways and modulating energy metabolism, both locally as well as over the whole cell.

SUPPORTING MATERIAL

Three appendices, six figures, and one table are available at http://www.biophysj.org/biophysj/supplemental/S0006-3495(09)01607-5.

REFERENCES

1. Bernardi, P. 1999. Mitochondrial transport of cations: channels, exchangers, and permeability transition. *Physiol. Rev.* 79:1127–1155.

2. Brookes, P. S., Y. Yoon, …, S. S. Sheu. 2004. Calcium, ATP, and ROS: a mitochondrial love-hate triangle. *Am. J. Physiol. Cell Physiol.* 287:C817–C833.

3. Duchen, M. R. 2000. Mitochondria and Ca^{2+} in cell physiology and pathophysiology. *Cell Calcium.* 28:339–348.

4. Gunter, T. E., K. K. Gunter, …, C. E. Gavin. 1994. Mitochondrial calcium transport: physiological and pathological relevance. *Am. J. Physiol.* 267:C313–C339.

5. O'Rourke, B., S. Cortassa, and M. A. Aon. 2005. Mitochondrial ion channels: gatekeepers of life and death. *Physiology (Bethesda).* 20:303–315.

6. Baysal, K., G. P. Brierley, …, D. W. Jung. 1991. Regulation of the mitochondrial Na^+/Ca^{2+} antiport by matrix pH. *Arch. Biochem. Biophys.* 291:383–389.

7. Paucek, P., and M. Jaburek. 2004. Kinetics and ion specificity of Na^+/Ca^{2+} exchange mediated by the reconstituted beef heart mitochondrial Na^+/Ca^{2+} antiporter. *Biochim. Biophys. Acta.* 1659:83–91.

8. Baysal, K., D. W. Jung, …, G. P. Brierley. 1994. Na^+-dependent Ca^{2+} efflux mechanism of heart mitochondria is not a passive $Ca^{2+}/2Na^+$ exchanger. *Am. J. Physiol.* 266:C800–C808.

9. Brand, M. D. 1985. The stoichiometry of the exchange catalyzed by the mitochondrial calcium/sodium antiporter. *Biochem. J.* 229:161–166.

10. Crompton, M., M. Capano, and E. Carafoli. 1976. The sodium-induced efflux of calcium from heart mitochondria. A possible mechanism for the regulation of mitochondrial calcium. *Eur. J. Biochem.* 69:453–462.

11. Crompton, M., M. Kunzi, and E. Carafoli. 1977. The calcium-induced and sodium-induced effluxes of calcium from heart mitochondria. Evidence for a sodium-calcium carrier. *Eur. J. Biochem.* 79:549–558.

12. Cox, D. A., and M. A. Matlib. 1993. A role for the mitochondrial Na^+-Ca^{2+} exchanger in the regulation of oxidative phosphorylation in isolated heart mitochondria. *J. Biol. Chem.* 268:938–947.

13. Jung, D. W., K. Baysal, and G. P. Brierley. 1995. The sodium-calcium antiport of heart mitochondria is not electroneutral. *J. Biol. Chem.* 270:672–678.

14. Kim, B., and S. Matsuoka. 2008. Cytoplasmic Na^+-dependent modulation of mitochondrial Ca^{2+} via electrogenic mitochondrial Na^+-Ca^{2+} exchange. *J. Physiol.* 586:1683–1697.

15. Wingrove, D. E., and T. E. Gunter. 1986. Kinetics of mitochondrial calcium transport. II. A kinetic description of the sodium-dependent calcium efflux mechanism of liver mitochondria and inhibition by ruthenium red and by tetraphenylphosphonium. *J. Biol. Chem.* 261:15166–15171.

16. Dash, R. K., and D. A. Beard. 2008. Analysis of cardiac mitochondrial Na^+-Ca^{2+} exchanger kinetics with a biophysical model of mitochondrial Ca^{2+} handling suggests a 3:1 stoichiometry. *J. Physiol.* 586:3267–3285.

17. Magnus, G., and J. Keizer. 1997. Minimal model of β-cell mitochondrial Ca^{2+} handling. *Am. J. Physiol.* 273:C717–C733.

18. Cortassa, S., M. A. Aon, …, B. O'Rourke. 2003. An integrated model of cardiac mitochondrial energy metabolism and calcium dynamics. *Biophys. J.* 84:2734–2755.

19. Nguyen, M. H., S. J. Dudycha, and M. S. Jafri. 2007. The effects of Ca^{2+} on cardiac mitochondrial energy production is modulated by Na^+ and H^+ dynamics. *Am. J. Physiol. Cell Physiol.* 292:2004–2020.

20. Keener, J. P., and J. Sneyd. 1998. Mathematical Physiology. Springer, New York.

21. Lauger, P. 1973. Ion transport through pores: a rate-theory analysis. *Biochim. Biophys. Acta.* 311:423–441.

22. Woodbury, J. W. 1971. Eyring rate theory model of the current-voltage relationship of ion channels in excitable membranes. *In* Chemical Dynamics: Papers in Honor of Henry Eyring. J. Hirschfelder, editor. John Wiley and Sons, New York.

23. Cornish-Bowden, A. 2004. Fundamentals of Enzyme Kinetics. Portland Press, London.

24. Metelkin, E., I. Goryanin, and O. Demin. 2006. Mathematical modeling of mitochondrial adenine nucleotide translocase. *Biophys. J.* 90:423–432.

25. Dash, R. K., F. Qi, and D. A. Beard. 2009. A biophysically based mathematical model for the kinetics of mitochondrial calcium uniporter. *Biophys. J.* 96:1318–1332.

26. Michailova, A., and A. McCulloch. 2001. Model study of ATP and ADP buffering, transport of Ca^{2+} and Mg^{2+}, and regulation of ion pumps in ventricular myocyte. *Biophys. J.* 81:614–629.

27. Bers, D. M. 2008. Calcium cycling and signaling in cardiac myocytes. *Annu. Rev. Physiol.* 70:23–49.

28. Wu, F., F. Yang, …, D. A. Beard. 2007. Computer modeling of mitochondrial tricarboxylic acid cycle, oxidative phosphorylation, metabolite transport, and electrophysiology. *J. Biol. Chem.* 282:24525–24537.